SUPPLEMENTARY INFORMATION FOR

Understanding the Origin of Disorder in Kesterite-type Chalcogenides A_2ZnBQ_4 (*A* = Cu, Ag; *B* = Sn, Ge; *Q* = S, Se): the Influence of Inter-layer Interactions.

Panagiotis Mangelis,[a] Alex Aziz,[a] Ivan da Silva Gonzalez,[b] Ricardo Grau-Crespo,[a] Paz Vaqueiro[a] and Anthony V. Powell[a]

[a] *Department of Chemistry, University of Reading, Whiteknights, Reading RG6 6AD, England, United Kingdom*

[b] *STFC, Rutherford Appleton Laboratory, ISIS Facility, Didcot OX11 0QX, United Kingdom*

S.1: Synthesis Procedure

The optimum synthetic procedure described below was established following exploratory synthesis in which a range of reaction temperatures and times were explored. The conditions presented are those which produce high-purity phases. $Cu_2ZnSnSe_4$, $Cu_2ZnGeSe_4$ and Cu_2ZnSnS_4 were prepared by heating the mixtures of elemental powders at 650 ˚C for 48 hours. The same reaction temperature was used to prepare Cu_2ZnGeS_4, although the heating time was extended 96 hours. The second firing of selenides was carried out at 800 ˚C for 96 hours. The synthesis of sulphides, Cu_2ZnSnS_4 and Cu_2ZnGeS_4, required a second firing for 96 hours at 850 ˚C and 700 ˚C respectively. A heating / cooling rate of 2 ˚C min^{-1} was applied in each firing of all compounds. For the synthesis of Ag_2ZnSnS_4 one firing was necessary at 650 ˚C for 96 hours with a heating / cooling rate of 0.5 ˚C min^{-1}. The corresponding selenide, $Ag_2ZnSnSe_4$, was prepared mechanochemically. Stoichiometric amounts of powdered elements were sealed, under an argon atmosphere, into a 25 mL stainless steel jar, together with thirty 6 mm diameter steel balls. The mixture was milled for 4 h at 600 rpm using a Retsch PM100 planetary ball mill and subsequently annealed at 500 °C for 30 min in an evacuated and sealed fused-silica tube.

S.2: Analysis of Powder X-ray Diffraction Data

All materials were initially analysed by powder X-ray diffraction. Rietveld refinements were carried out for all materials in the space groups *I*-4 and *I*-42*m*. Following the refinement of the scale factor, the background parameters were refined using the reciprocal interpolation function. Subsequently, zero point, lattice parameters, atomic coordinates of the anions and thermal parameters were introduced into the refinement. The peak shape was modelled using a pseudo-Voigt function which mixes Gaussian and Lorentzian functions. Initial refinement of cation site occupancy factors was carried out without constraints, using the idealized fully ordered structural model for each structure type. Site occupancy factors showed no significant deviation from full occupancy and they were subsequently fixed at unity.

S.3 Band structures and band gaps

Table S1 presents the calculated band gaps for all the compositions included in this study, as obtained for the **K1** and **K2** configurations using the HSE functional, in comparison with available experimental values. The substitution of S with Se tends to decrease the band gap, whereas the substitution of Cu with Ag tends to increase the band gap. These trends are consistent with experiment, as shown in the table. The band gap values calculated for **K1** and **K2** configurations are similar, except in the Ag-based materials, where only the K1 configuration is relevant due to the high degree of ordering.

Table S1. Band gaps calculated for different compositions of the A_2BCX_4 system in the K1 and K2 configurations (eV)

	K1	K2	Experiment
CZGS	2.09	2.04	1.88–2.20[1.2]
CZGSe	1.26	1.17	1.40–1.43[1]
CZTS	1.49	1.46	1.47 - 1.51 [3-11]
CZTSe	0.91	0.88	0.97-1.04 [12-14]
AZTS	1.74	1.56	2.00[2]
AZTSe	1.08	0.92	1.40[15]

1. Khadka, D.B. and J.H. Kim, *Study of structural and optical properties of kesterite Cu2ZnGeX4 (X = S, Se) thin films synthesized by chemical spray pyrolysis.* CrystEngComm, 2013. **15**(48): p. 10500-10509.
2. Tsuji, I., et al., *Novel Stannite-type Complex Sulfide Photocatalysts A(2)(I)-Zn-A(IV)-S-4 (A(I) = Cu and Ag; A(IV) = Sn and Ge) for Hydrogen Evolution under Visible-Light Irradiation.* Chemistry of Materials, 2010. **22**(4): p. 1402-1409.
3. Katagiri, H., et al., *Development of thin film solar cell based on Cu2ZnSnS4 thin films.* Solar Energy Materials and Solar Cells, 2001. **65**(1-4): p. 141-148.
4. Green, M.A., et al., *Solar cell efficiency tables (version 46).* Progress in Photovoltaics, 2015. **23**(7): p. 805-812.
5. Kamoun, N., H. Bouzouita, and B. Rezig, *Fabrication and characterization of Cu2ZnSnS4 thin films deposited by spray pyrolysis technique.* Thin Solid Films, 2007. **515**(15): p. 5949-5952.
6. Tanaka, T., et al., *Preparation of Cu2ZnSnS4 thin films by hybrid sputtering.* Journal of Physics and Chemistry of Solids, 2005. **66**(11): p. 1978-1981.
7. Seol, J.S., et al., *Electrical and optical properties of Cu2ZnSnS4 thin films prepared by rf magnetron sputtering process.* Solar Energy Materials and Solar Cells, 2003. **75**(1-2): p. 155-162.
8. Scragg, J.J., et al., *New routes to sustainable photovoltaics: evaluation of Cu2ZnSnS4 as an alternative absorber material.* Physica Status Solidi B-Basic Solid State Physics, 2008. **245**(9): p. 1772-1778.
9. Sekiguchi, K., et al., *Epitaxial growth of Cu2ZnSnS4 thin films by pulsed laser deposition*, in *Physica Status Solidi C*, M. Stutzmann, Editor. 2006. p. 2618-2621.
10. Nakayama, N. and K. Ito, *Sprayed films of stannite Cu2ZnSnS4.* Applied Surface Science, 1996. **92**: p. 171-175.
11. Zhang, J., et al., *Cu2ZnSnS4 thin films prepared by sulfurization of ion beam sputtered precursor and their electrical and optical properties.* Rare Metals, 2006. **25**: p. 315-319.
12. Brammertz, G., et al., *Characterization of defects in 9.7% efficient Cu2ZnSnSe4-CdS-ZnO solar cells.* Applied Physics Letters, 2013. **103**(16): p. 163904.
13. Choi, S.G., et al., *Temperature dependent band-gap energy for Cu2ZnSnSe4: A spectroscopic ellipsometric study.* Solar Energy Materials and Solar Cells, 2014. **130**: p. 375-379.
14. Giraldo, S., et al., *Large Efficiency Improvement in Cu2ZnSnSe4 Solar Cells by Introducing a Superficial Ge Nanolayer.* Advanced Energy Materials, 2015. **5**(21): p. 1501070.
15. Wei, K. and G.S. Nolas, *Synthesis and Characterization of Nanostructured Stannite Cu2ZnSnSe4 and Ag2ZnSnSe4 for Thermoelectric Applications.* ACS Applied Materials & Interfaces, 2015. **7**(18): p. 9752-9757.

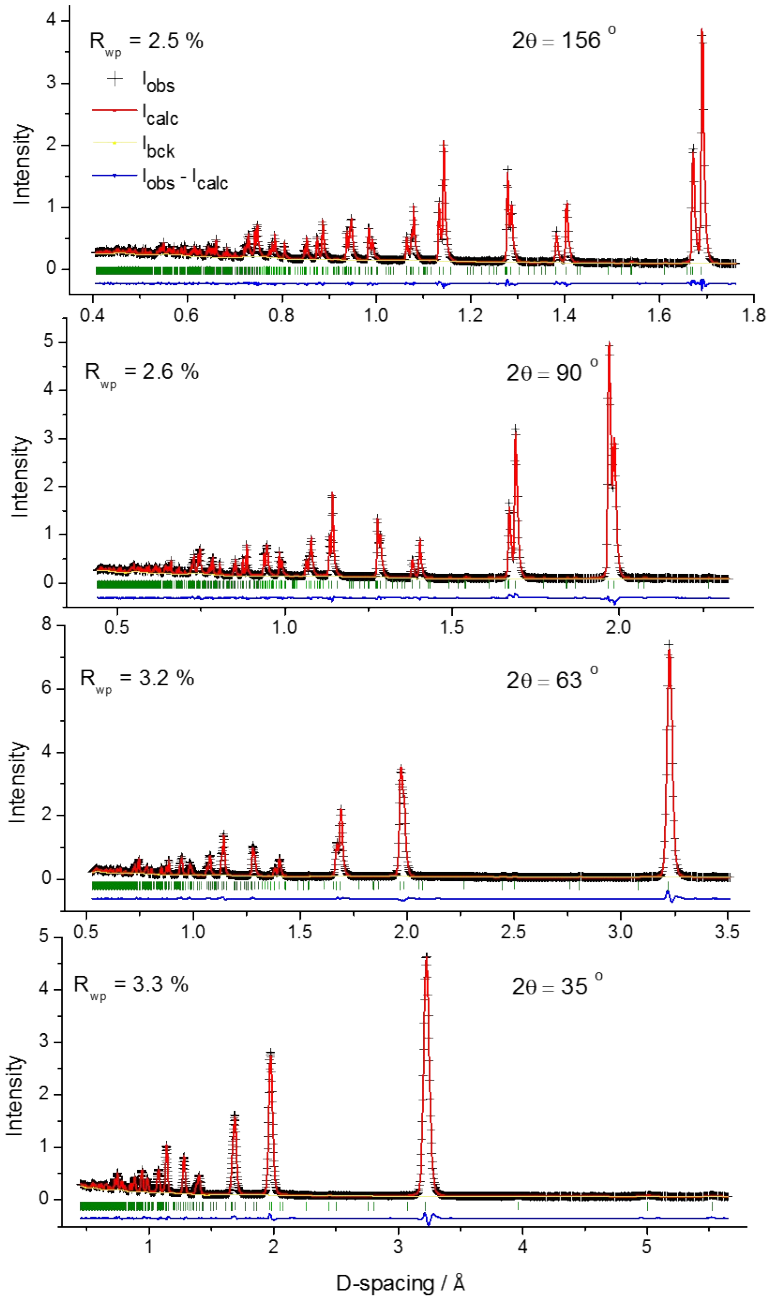

Figure S1 Multibank Rietveld refinement for $Cu_2ZnGeSe_4$ using powder neutron diffraction data collected at room temperature. Observed (black crosses), refined (red solid lines), difference (lower blue line) profiles. Reflection positions are marked by olive lines.

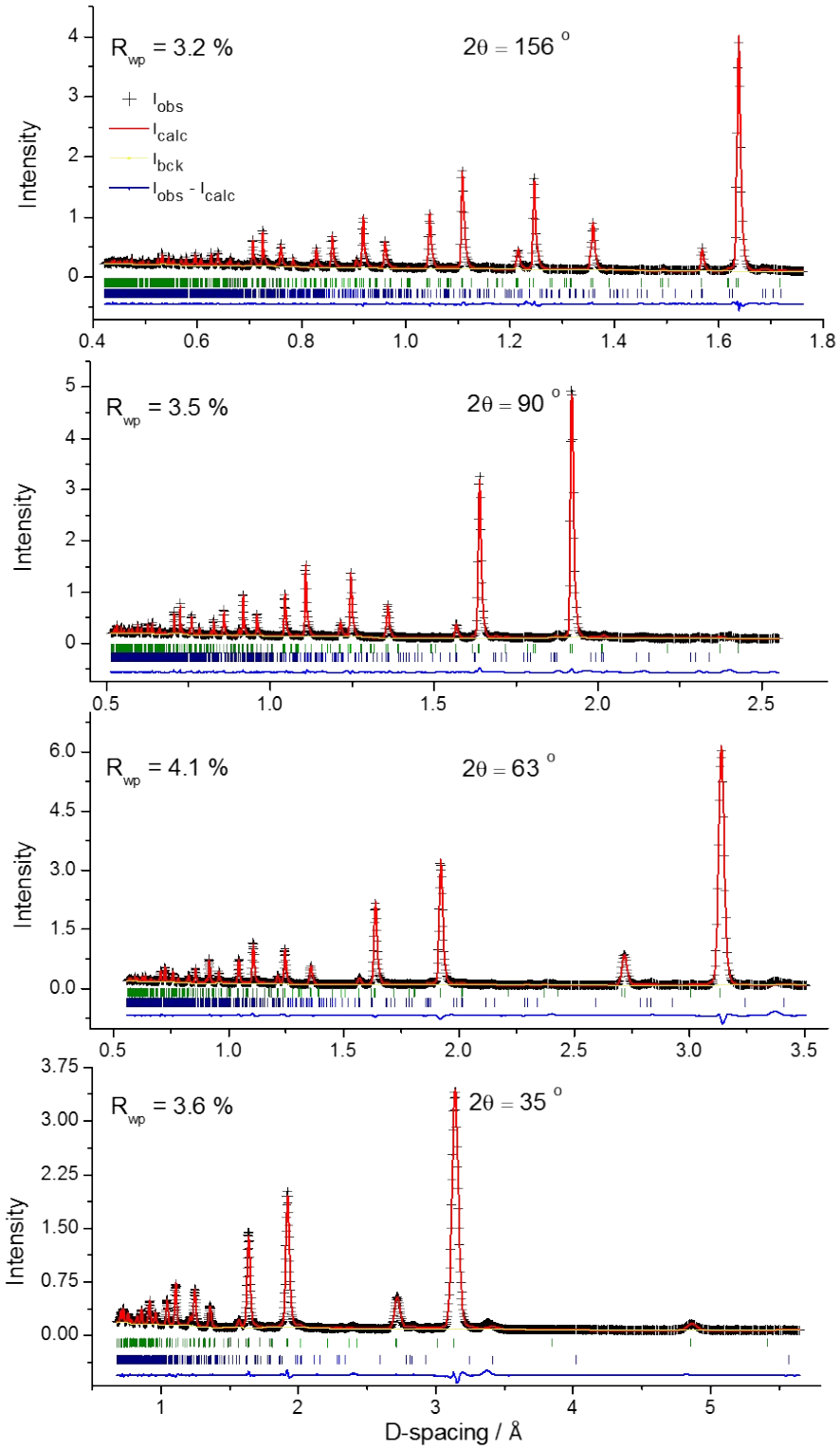

Figure S2 Multibank Rietveld refinement for Cu_2ZnSnS_4 using powder neutron diffraction data collected at room temperature. Observed (black crosses), refined (red solid lines), difference (lower blue line) profiles. Reflection positions of the Cu_2ZnSnS_4 phase are indicated by olive markers, while navy markers denote SnS.

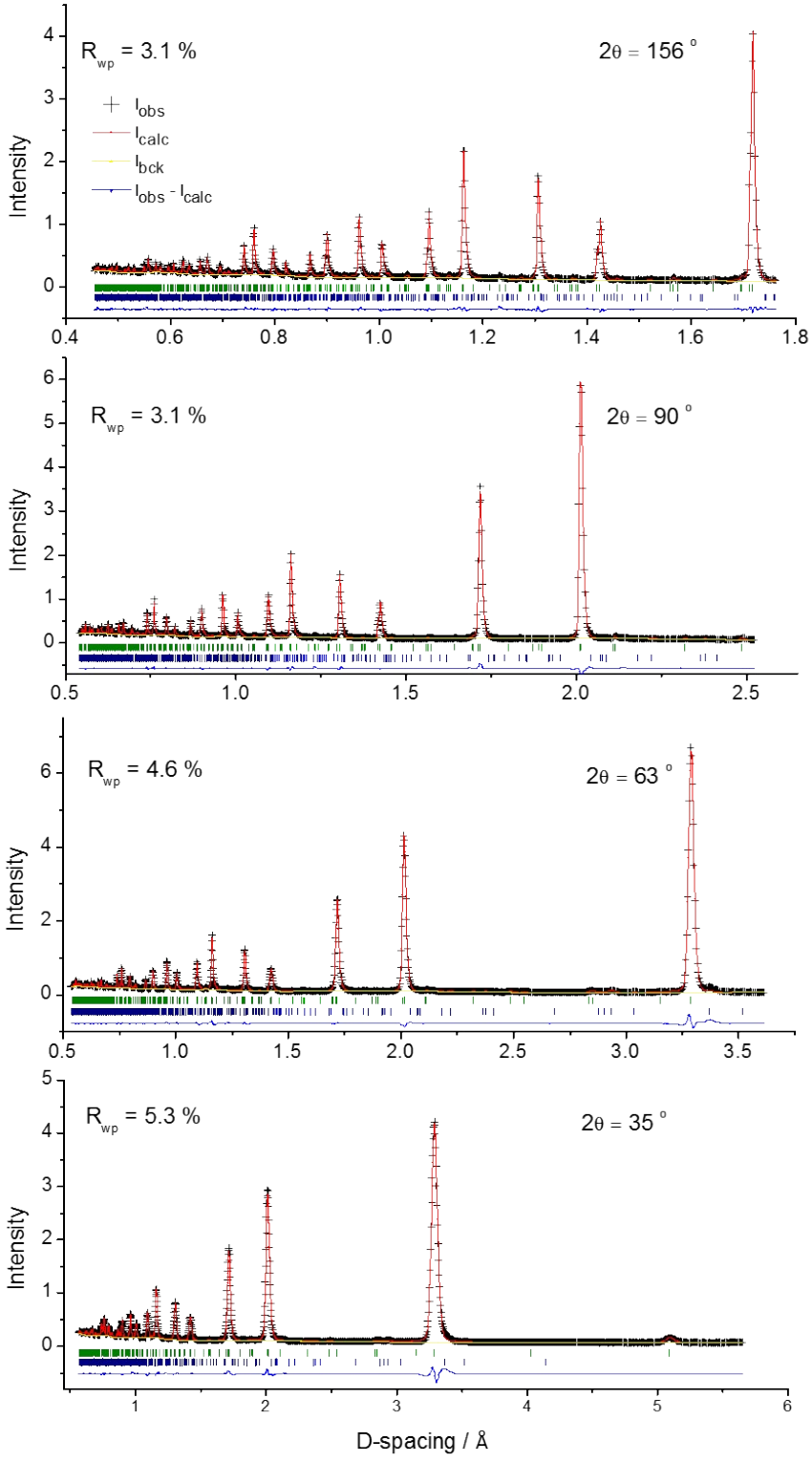

Figure S3 Multibank Rietveld refinement for $Cu_2ZnSnSe_4$ using powder neutron diffraction data collected at room temperature. Observed (black crosses), refined (red solid lines), difference (lower blue line) profiles. Reflection positions of the $Cu_2ZnSnSe_4$ phase are indicated by olive markers, while navy markers denote SnSe.

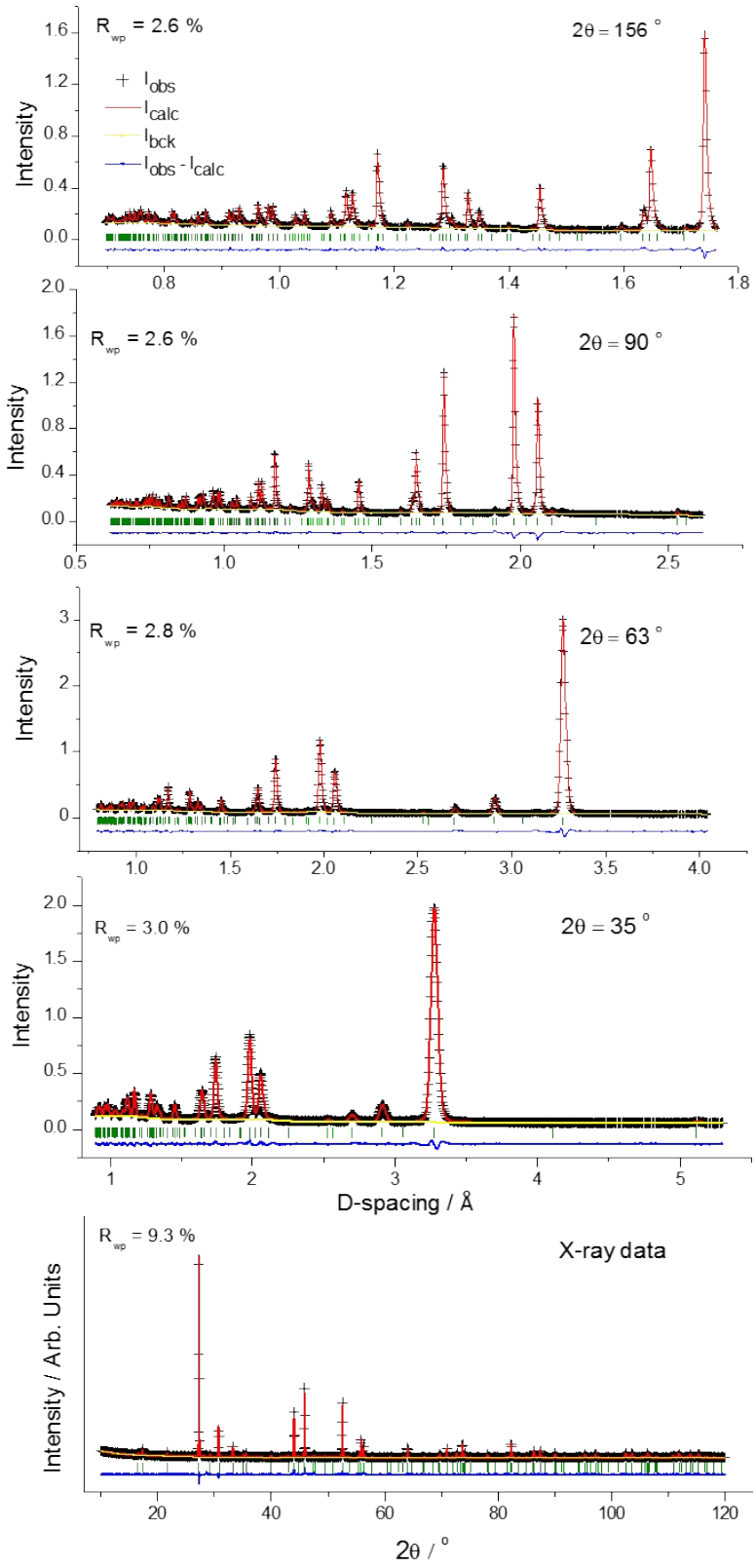

Figure S4 Multibank Rietveld refinement for Ag_2ZnSnS_4 combining powder neutron and X-ray diffraction data collected at room temperature. Observed (black crosses), refined (red solid lines), difference (lower blue line) profiles. Reflection positions are marked by olive lines.

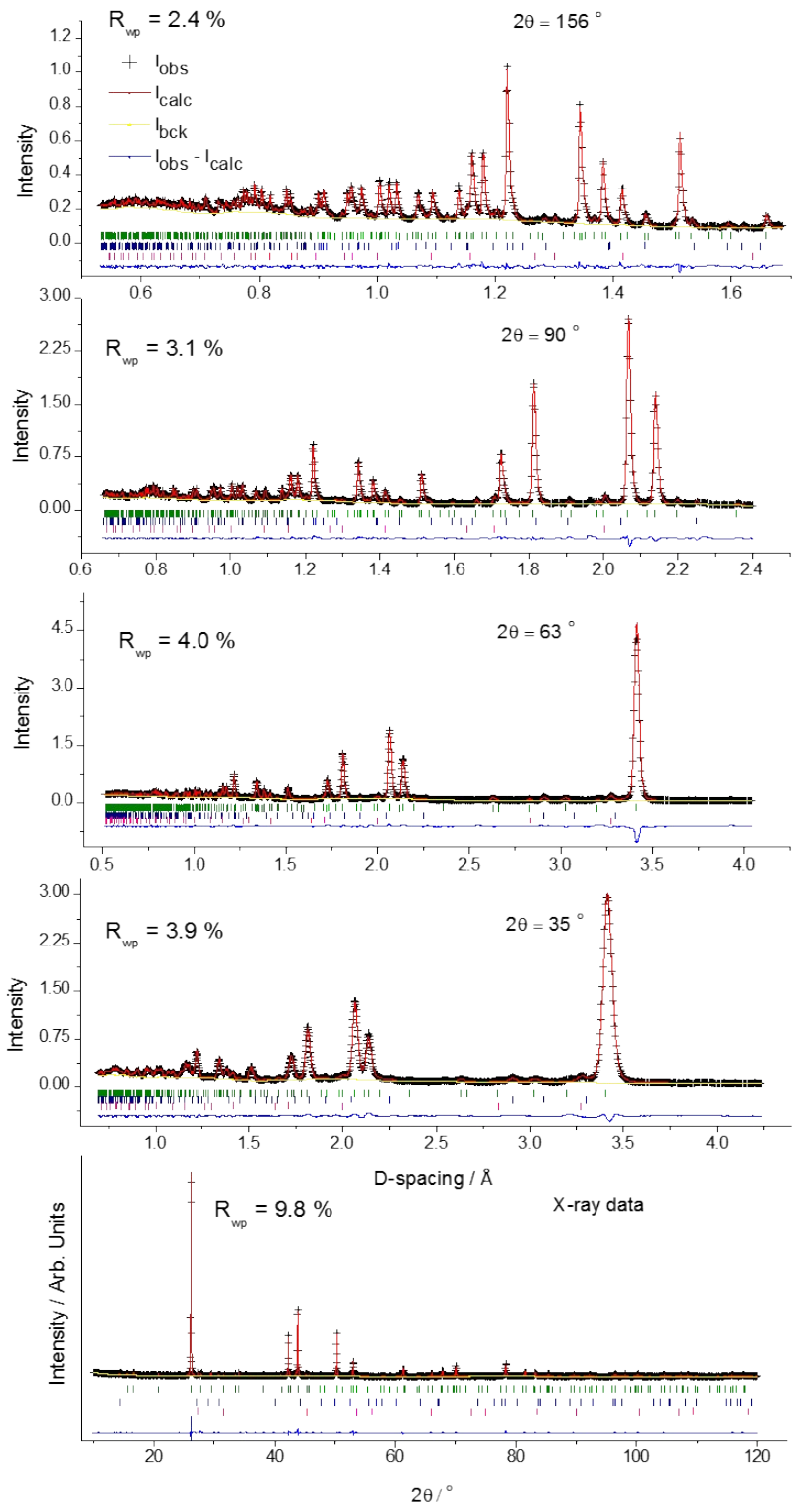

Figure S5 Multibank Rietveld refinement for $Ag_2ZnSnSe_4$ combining powder neutron and X-ray diffraction data collected at room temperature. Observed (black crosses), refined (red solid lines), difference (lower blue line) profiles. Reflection positions of $Cu_2ZnSnSe_4$ phase are indicated by olive markers, while navy and pink markers denote SnSe and ZnSe respectively.